Available online at www.sciencedirect.com
SCIENCE DIRECT®
ELSEVIER
Nuclear Instruments and Methods in Physics Research B 216 (2004) 100–104
NIM B
Beam Interactions with Materials & Atoms
www.elsevier.com/locate/nimb

Atomistic analysis of the ion beam induced defect evolution

Maria Aboy *, Lourdes Pelaz, Luis A. Marqués, Juan Barbolla

Campus Miguel Delibes, University of Valladolid, 47011 Valladolid, Spain

Abstract

Kinetic non-lattice Monte Carlo atomistic simulations are used to analyze the ion beam induced defect evolution. This is studied in terms of the probabilities of emitted interstitials being recaptured by other defects or in turn, being annihilated at the surface. In this way, the ripening and dissolution of interstitial defects can be explained as a competition between the average distance among defects and their distance to the surface, that acts as an efficient sink. At the beginning of the anneal Si interstitials are mostly exchanged among defects, with a minimal loss of them through diffusion to the surface. This leads to the formation of larger defects at the expense of the smaller ones. As their size increases and the defect dose decreases, the average distance among them increases. Then, the loss of Si interstitials through diffusion to the surface prevails, causing their dissolution. The presence of large and stable defects near the surface is also possible in low energy implants if the dose is high enough.

PACS: 61.80.Az; 82.20.Wt; 67.80.Mg; 61.72.Ji
Keywords: Modeling; Silicon; Defects; Ripening

1. Introduction

Ion beam processing is the most standard technique used to introduce dopants in silicon for the fabrication of integrated circuits. However, this process produces considerable damage in the Si lattice, and generates defects that might degrade the device performance. Therefore, a postimplant thermal process is necessary to recover the lattice. Frenkel pairs generated in each implantation cascade are annealed out quickly, leaving one Si interstitial per implanted ion which can not be annealed out immediately (“+1” model [1]). This excess of Si interstitials condenses into small clusters, {3 1 1} defects and dislocation loops [2,3], sustaining a local supersaturation of interstitials by emitting and recapturing interstitials during annealing. The Si interstitial defects dissolve by a gradual loss of interstitials from the damage region through diffusion to the surface.

The role of the surface in the removal of point defects has been studied by several authors [4–6]. Venezia et al. [4] reported a linear dependence of the dissolution time of the {3 1 1} defects with depth. Agarwal et al. [5] showed that large and stable {3 1 1} defects were observed for 5 keV Si implants, despite the proximity to the surface. Moller et al. [6] suggested that the surface does not play a key role in the interstitial removal from

* Corresponding author. Tel.: +34-983423683x5504; fax: +34-983423675.
E-mail address: marabo@tel.uva.es (M. Aboy).

0168-583X/$ - see front matter © 2003 Elsevier B.V. All rights reserved.
doi:10.1016/j.nimb.2003.11.027

{3 1 1} defects during the annealing, since the defect layer does not change considerably until the {3 1 1} defects nearly completely dissolve.

2. Simulation model

We use kinetic Monte Carlo simulations to analyze the role of surface in Si interstitial defect dissolution. For our study, we carried out atomistic simulations with the following scheme: the implantation cascades are generated with the binary collision computer code MARLOWE [7], and the coordinates of the resulting Si self-interstitials and vacancies are transferred to the kinetic non-lattice Monte Carlo diffusion code DADOS [8]. The binding energies used in the non-lattice kinetic Monte Carlo simulations, are obtained from ab initio calculations or estimated by fitting experimental data [2,3]. The migration and formation energies for Si self-interstials are taken from [9]. For small Si interstitial clusters ($n < 10$) we take the oscillating formation energies experimentally deduced by Cowern et al. [3] For larger sizes, we use the experimental binding energy of {1 1 3} defects [2,3]. No loops are formed in the experiments under study. The surface is considered as an efficient sink for point defects, with a recombination length $L < 20$ nm [10].

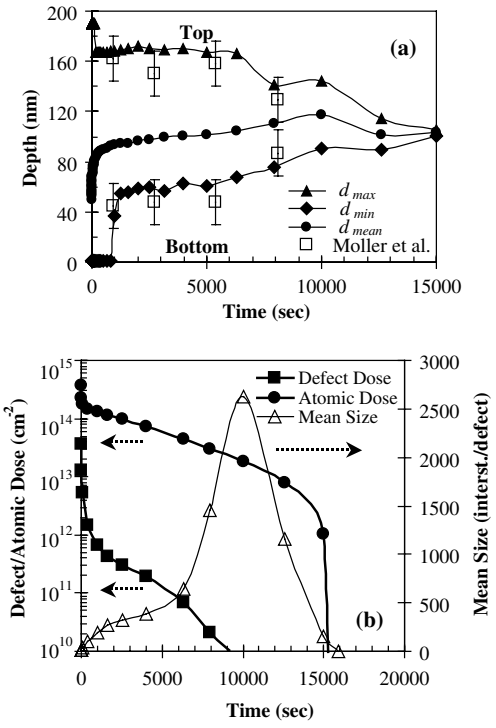

Fig. 1. (a) Time evolution of the top (d_{max}), the bottom (d_{min}) and the mean (d_{mean}) position of the Si interstitials in the defect layer, for a simulated 40 keV Si implant with a dose of 10^{14} ions/cm^2. Experimental data from Moller et al. [6] are also plotted. (b) Time evolution during annealing at 750 °C of the atomic and defect dose of Si interstitials in defects. Time evolution of the mean size of the defects is also plotted.

3. Time evolution of a layer of Si interstitial defects

We have investigated the mechanism of the removal of Si interstitials from the top and the bottom of a layer of {3 1 1} defects and the role of the surface. We have simulated the implantation of 40 keV Si ions, to a dose of 10^{14} cm^{-2}, annealed at 750 °C, as in an experiment by Moller et al. [6]. Fig. 1 plots the simulated time evolution of the top and the bottom positions of the Si interstitial defect layer, and also the results reported by Moller et al. In the simulation, the top and the bottom of the defect layer are defined as the positions of the Si interstitials in defects placed the closest and furthest to the surface, respectively. The simulation shows that the defect layer width remains almost unchanged for about 6000 s, similarly to the experiments. The positions of the top and the bottom of the defect layer remains almost the same until the {3 1 1} defects nearly completely dissolve, and it does not seem to have preferential annihilation near the surface. This behavior could suggest that the defect dissolution is not controlled by the surface annihilation. However, in the simulations the surface is considered as an efficient sink for point defects. Therefore, the experimental results reported by Moller et al. are compatible with the fact that the surface controls the dissolution of Si interstitial defects.

To analyze in more detail the evolution of damage during the postimplant anneal, we have plotted in Fig. 1(b) the simulated time evolution of the dose of Si interstitials, the dose of the interstitial defects and also the mean size of these

defects. Several stages can be distinguished in the temporal evolution of the Si interstitial defects. During the ramp up, and at the very early stages of the annealing, there is a high concentration of Si interstitials, and also, a high concentration of vacancies generated by the implantation. The sudden drop in the Si interstitial dose at the beginning of the annealing in Fig. 1(b) corresponds to the quick recombination of interstitials with vacancies. At ~60 s of the annealing, the vacancies are annihilated. This leaves approximately one Si interstitial per implanted ion which cannot be annealed out with the corresponding vacancies (dose $\sim 10^{14}$ cm^{-2}). As the anneal proceeds, the "+1" interstitials condense into small interstitial clusters and {3 1 1} defects. Fig. 1(b) shows that during a long period of time (~6000 s), the interstitial dose remains almost constant ($\sim 10^{14}$ cm^{-2}) as very few interstitials are lost to the surface. During this period of time, the mean size of the defects increases by the exchange of interstitials among them, at the same time that the defect dose decreases (see Fig. 1(b)). Once the mean size of the defects has reached a large value, and the defect dose is low, the Si interstitial dose held in the Si interstitial defects decreases quickly as many interstitials are lost through diffusion to the surface.

This could be explained by the random-walk theory [11], and is schematized in Fig. 2. At the first stages of annealing, when there are many small defects, the distance among them is much shorter than the distance to the surface. Therefore, emitted Si interstitials are more likely to be recaptured by another defect than to reach the surface. In this way, interstitials are emitted from and recaptured by the defects, favoring the growth of larger and more stable defects at the expense of smaller ones (Ostwald ripening). As the average size of the defects increases during the ripening, the density of defects decreases, in order to keep approximately constant the density of Si interstitials,

$$\text{Atomic\_Dose} = \text{Defect\_Dose} \times \text{Mean\_Size}. \quad (1)$$

Therefore, the average distance among the defects, d_{def}, increases as the defect dose decreases, since

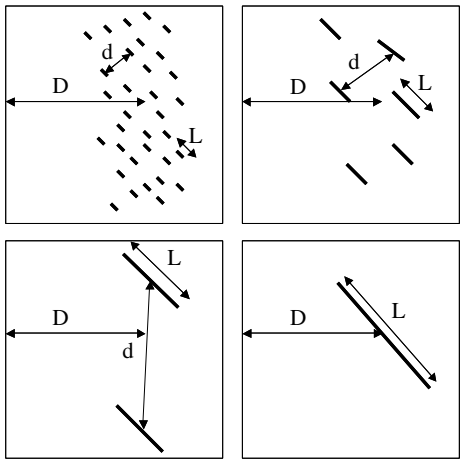

Fig. 2. Schematic of the time evolution of a layer of {3 1 1} defects during its ripening and dissolution. Defects evolve to larger sizes, at the expense of the smaller ones, while the distance among defects, d, is smaller than the distance to the surface, D. The probability of an emitted Si interstitial to be recaptured by another defect is larger than to reach the surface. When the defects grow to large sizes, the defect dose is low and the distance among defects becomes comparable to the distance to the surface, and these two probabilities become comparable. Then, the dissolution of Si interstitial defects takes place quickly.

the mean distance among defects can be estimated by

$$d_{\text{def}} = \sqrt[3]{\frac{d_{\max} - d_{\min}}{\text{Defect\_Dose}}}, \quad (2)$$

where $d_{\max} - d_{\min}$ is the width of the defect layer. Then, when the distance among defects becomes comparable to the distance to the surface, the probability of interstitials being recaptured in the layer becomes comparable to the probability of them being annihilated at the surface. At this point, as the exchange of interstitials continues, a significant number of Si interstitials are lost by recombination at the surface. The defect dose decreases further, the distance among defects increases and, consequently, the probability of interstitials being annihilated at the surface increases. This results in the quick dissolution of Si interstitial defects at the final stages of the annealing.

In order to apply this reasoning to our simulation results, we extracted the values of the Si

interstitial defect dose and the defect layer width corresponding to the instant in which the defect layer shrinks (~6000 s, as is seen in Fig. 1(a)). These values were 7×10^{10} cm^{-2} and 100 nm, respectively. The estimated mean distance among defects is then about 50 nm, which is comparable to the distance of the defect layer to the surface. Then, from this instant of the annealing, there is a no negligible probability of a Si interstitial, even from the top region, to go through the layer and to reach the surface, and both sides of the defect layer shrink. Nevertheless, note that the mean position slightly shifts towards deeper positions.

4. {3 1 1} defects from low energy and high dose implants

Despite the proximity to the surface, large and very stable defects near the surface were observed for a 5 keV Si implant, annealed at 750 °C [5]. Moreover, a superlinear increase in their size and stability is observed when going from implantation doses of 10^{14} to 3×10^{14} ions/cm^2. The simulation results show similar behavior, as can be seen in Fig. 3, where we plot the maximum defect size for 5 keV Si implants with doses of 10^{14}, 2×10^{14} and 3×10^{14} ions/cm^2, annealed at 750 °C. The defect size increases with implantation dose, with a large

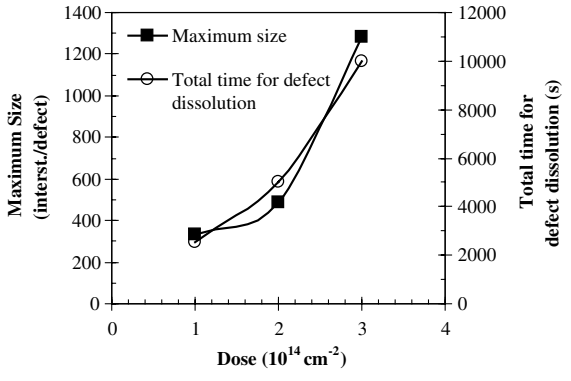

Fig. 3. Implantation dose dependence of the maximum size and the total time of existence of interstitial defects for 5 keV Si implants, annealed at 750 °C. A sharp increase is observed when going from 2×10^{14} cm^{-2} to 3×10^{14} cm^{-2}.

rise in size when going from 2×10^{14} to 3×10^{14} ions/cm^2. The formation of these long and stable defects is related to the high concentration of excess interstitials that appears for the high dose implant. This leads to a significant reduction in the average distance among defects within the defect layer. Therefore, interstitials emitted from defects are likely to be recaptured despite the proximity to the surface, and larger defects can be formed. From the simulations, we obtain a superlinar increase in the duration of Si interstitial defects with the implantation dose, as is observed in the experiments too.

The previously explained competition between the average distance among defects and the distance to the surface, does not explain the superlinearity with dose that appears in the size and stability of defects for these low energy implants. It is expected a linear dependence, according to [12] and Eq. (1). To explain this anomalous behavior for the 3×10^{14} ions/cm^2, 5 keV Si implant, we have analyzed in more detail the ripening of the defects during annealing. The average distance among defects is estimated using Eq. (2), with Defect_Dose and $d_{\max} - d_{\min}$ extracted from the simulations. The average length of the defects is extracted from the simulated Mean_Size (average number of interstitials per defect), using an average number of 25 interstitials per nm of length, as is measured experimentally [13]. The time evolution of both magnitudes for the 2×10^{14} and the 3×10^{14} ions/cm^2 doses, respectively, is plotted in Fig. 4(a) and (b). For the 10^{14} ions/cm^2 case, the obtained evolution is similar to the one for the 2×10^{14} ions/cm^2 case, but the average length of the defects is even smaller. For the low dose case, the length of the defects is smaller than both the distance to the surface (~10 nm) and the distance among defects, during all the annealing time. However, for the high dose case, the size of the defects becomes such that their average length exceeds the distance to the surface, and can even be larger than the average distance among defects. The long defects have larger capture radius, favoring the recapture of the emitted Si interstitials. Also interactions between {3 1 1} defects with different orientations could lead to the formation of more stable structures.

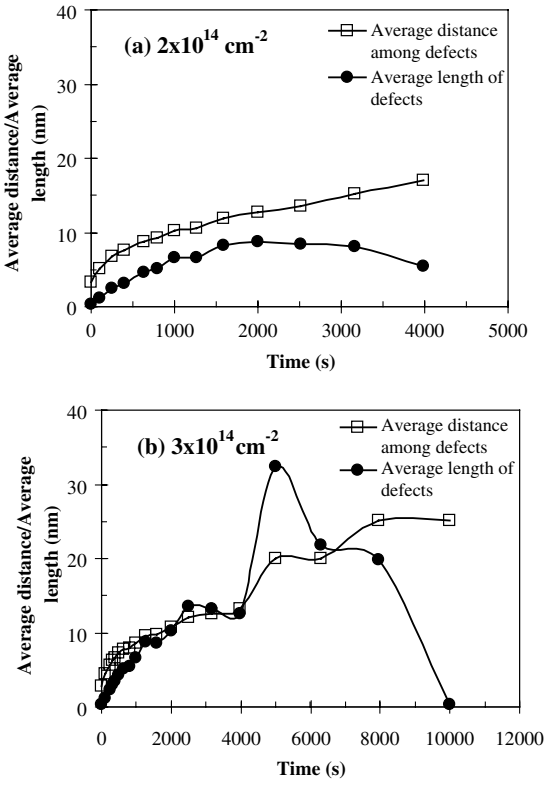

Fig. 4. Time evolution of the average distance among defects and average length of defects, extracted from the simulations of 5 keV implants with implantation doses of (a) 2×10^{14} cm^{-2} and (b) 3×10^{14} cm^{-2}, and annealed at 750 °C. In the lower dose case, the average distance among defects is always smaller than the average length of the defects, while in the higher dose case, the average length of the defects can be even larger than the average distance among defects.

5. Conclusions

We have used atomistic kinetic Monte Carlo techniques to analyze the Si interstitial defect evolution. We have shown that the defect dissolution during the postimplant annealing is controlled by the annihilation of Si interstitials at the surface. This is compatible with experiments, which indicate that both sides of a {1 1 3} layer do not change considerably until the defects nearly completely dissolve, and the position of the bottom of the {1 1 3} layer does not exhibit preferential annihilation. Also, the formation of stable defects close to the surface in low energy implants is possible if the implantation dose is high enough.

References

[1] M. Giles, J. Electrochem. Soc. 138 (1991) 1160.
[2] D.J. Eaglesham, P.A. Stolk, H.-J. Gossmann, J.M. Poate, Appl. Phys. Lett. 65 (1994) 2305.
[3] N.E.B. Cowern, G. Mannino, P.A. Stolk, F. Roozeboom, H.G.A. Huizing, J.G.M. van Berkum, W.B. de Boer, F. Cristiano, A. Claverie, M. Jaraiz, Phys. Rev. Lett. 82 (1999) 4460.
[4] V.C. Venezia, R. Kalyanaraman, H.-J. Gossmann, C.S. Rafferty, P. Werner, Appl. Phys. Lett. 79 (2001) 1429.
[5] A. Agarwal, H.-J. Gossmann, D.J. Eaglesham, L. Pelaz, S.B. Herner, D.C. Jacobson, T.E. Haynes, R. Simonton, Mater. Sci. Semicond. Process. 1 (1998) 17.
[6] K. Moller, K.S. Jones, M.E. Law, Appl. Phys. Lett. 72 (1998) 2547.
[7] M.T. Robinson, I.M. Torrens, Phys. Rev. B 9 (1974) 5008.
[8] M. Jaraiz, L. Pelaz, J.E. Rubio, J. Barbolla, G.H. Gilmer, D.J. Eaglesham, H.-J. Gossmann, J.M. Poate, Mater. Res. Soc. Sympos. Proc. 532 (1998) 43.
[9] H. Bracht, E.E. Haller, R. Clark-Phelps, Phys. Rev. Lett. 81 (1998) 393.
[10] N.E.B. Cowern, D. Alquier, M. Omri, A. Claverie, A. Nejim, Nucl. Instr. and Meth. B 148 (1999) 257.
[11] For example D.R. Olander, Fundamental Aspects of Nuclear Reactor Fuel Elements, ERDA, Technical Information Center, Oak Ridge, Tennesee, 1976, Chapter 7.
[12] C.S. Rafferty, G.H. Gilmer, M. Jaraiz, D. Eaglesham, H.-J. Gossmann, Appl. Phys. Lett. 68 (1996) 2395.
[13] S. Takeda, Jpn. J. Appl. Phys. 1 30 (1991) L639.